NANO LETTERS

Letter

Electrical Manipulation of Nanofilaments in Transition-Metal Oxides for Resistance-Based Memory

Myoung-Jae Lee, Seungwu Han, Sang Ho Jeon, Bae Ho Park, Bo Soo Kang, Seung-Eon Ahn, Ki Hwan Kim, Chang Bum Lee, Chang Jung Kim, In-Kyeong Yoo, David H. Seo, Xiang-Shu Li, Jong-Bong Park, Jung-Hyun Lee, and Youngsoo Park

Nano Lett., **2009**, 9 (4), 1476-1481• DOI: 10.1021/nl803387q • Publication Date (Web): 18 March 2009

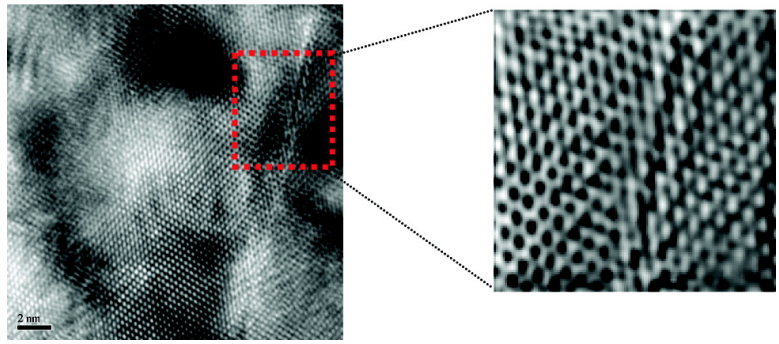

More About This Article

Additional resources and features associated with this article are available within the HTML version:

- Supporting Information
- Access to high resolution figures
- Links to articles and content related to this article
- Copyright permission to reproduce figures and/or text from this article

View the Full Text HTML

Nano Letters is published by the American Chemical Society. 1155 Sixteenth Street N.W., Washington, DC 20036

NANO LETTERS

2009
Vol. 9, No. 4
1476-1481

Electrical Manipulation of Nanofilaments in Transition-Metal Oxides for Resistance-Based Memory

Myoung-Jae Lee,*,† Seungwu Han,*,‡ Sang Ho Jeon,§ Bae Ho Park,§ Bo Soo Kang,† Seung-Eon Ahn,† Ki Hwan Kim,† Chang Bum Lee,† Chang Jung Kim,† In-Kyeong Yoo,† David H. Seo,|| Xiang-Shu Li,† Jong-Bong Park,† Jung-Hyun Lee,† and Youngsoo Park†

Samsung Advanced Institute of Technology, Samsung Electronics Co., Ltd. San 14-1, Yongin-si, Gyeonggi-Do, 446-712, Korea, Department of Physics, Ewha Womans University, Seoul 120-750, Korea, Division of Quantum Phases & Devices, School of Physics, Konkuk University, Seoul 143-701, Korea, and Department of Materials Science and Engineering, Stanford University, Palo Alto, California 94305

Received November 9, 2008; Revised Manuscript Received February 10, 2009

ABSTRACT

The fabrication of controlled nanostructures such as quantum dots, nanotubes, nanowires, and nanopillars has progressed rapidly over the past 10 years. However, both bottom-up and top-down methods to integrate the nanostructures are met with several challenges. For practical applications with the high level of the integration, an approach that can fabricate the required structures locally is desirable. In addition, the electrical signal to construct and control the nanostructures can provide significant advantages toward the stability and ordering. Through experiments on the negative resistance switching phenomenon in Pt−NiO−Pt structures, we have fabricated nanofilament channels that can be electrically connected or disconnected. Various analyses indicate that the nanofilaments are made of nickel and are formed at the grain boundaries. The scaling behaviors of the nickel nanofilaments were closely examined, with respect to the switching time, power, and resistance. In particular, the 100 nm × 100 nm cell was switchable on the nanosecond scale, making them ideal for the basis for high-speed, high-density, nonvolatile memory applications.

Nature offers various systems that can exist in two or more stable states. In particular, solid-state systems that can be cyclically transformed by an electrical signal have provided the promise of high-performance, high-density memories.[1−3] The current technology that based on charge storage, such as flash memory, has become increasingly limited as the cell size decreases and the total number of stored charges approach just a few electrons. The nanotubes and nanowires are certainly promising components in the high-density memories that can overcome the limitation of the current silicon technology.[4−7] However, the bottom-up or top-down approach that is necessary to integrate the nanostructure is met with many hurdles; in the bottom-up technique, it is difficult to achieve the position controlling of nanostructures, which is essential for the fabrication of high-density arrays required in commercial applications.[8] On the other hand, the most top-down approaches exploit the electron-beam lithography that has a low throughput and high cost. In addition, the mandatory etching step may damage the fragile nanostructures.

Recently, the resistance-switching phenomena of transition-metal oxides have been attracting many interests, because it can provide a basic principle of the next-generation nonvolatile memory.[1,3,9] There are several advantages in using transition-metal oxides. First, because of a relatively simple composition, the metal oxide can be deposited using the conventional techniques such as chemical or physical vapor deposition methods. Second, thin films of transition-metal oxides exhibit resistance switching in the polycrystalline state. This improves the device uniformity, because it can reduce the sensitivity to various deposition conditions such as substrate orientations. Third, the stoichiometry of oxide thin films can be adjusted over a relatively wide range of values during growth, allowing for a detailed control of film properties in a manner similar to the techniques currently applied for optoelectronic devices.[9,10] Lastly, as will be shown in the below, the nanoscale filament can be formed by the

* Author to whom correspondence should be addressed. E-mail: myoungjae.lee@samsung.com (M.-J.L.), hansw@ewha.ac.kr (S.H.).

† Samsung Advanced Institute of Technology, Samsung Electronics Co., Ltd.

‡ Department of Physics, Ewha Womans University.

§ Division of Quantum Phases & Devices, School of Physics, Konkuk University.

|| Department of Materials Science and Engineering, Stanford University.

10.1021/nl803387q CCC: $40.75
Published on Web 03/18/2009

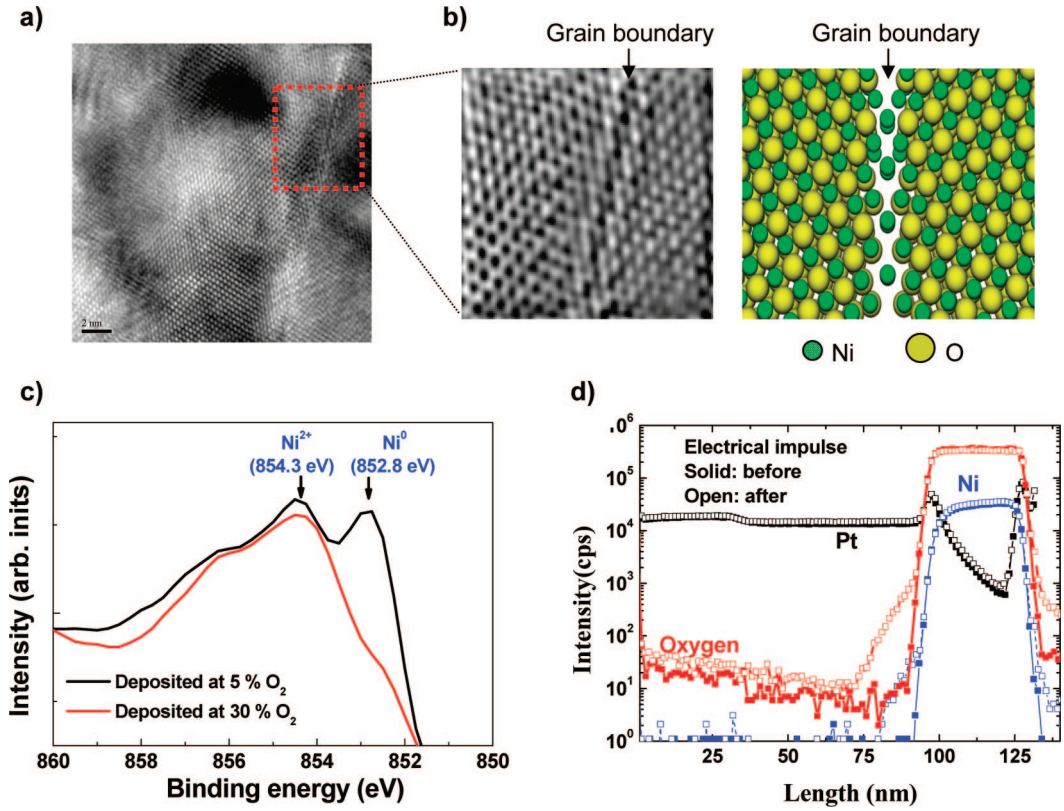

Figure 1. (a) High-resolution transmission electron microscopy (HR-TEM) image of the NiO layer, which shows the electrical switching behavior; crystalline order can be seen in the bulk of grains, and scale bar represents 2 nm. (b) Left panel shows an inverse fast Fourier transform (IFFT) transmission electron microscopy (TEM) image of the boxed area in panel (a), showing the grain-boundary region; the right side is a schematic drawing of the grain boundary in NiO, showing the location of the cations (small and green spheres) and anions (large and yellow spheres). Nickel nanofilament precipitates are present at the grain boundary. (c) X-ray photoelectron spectroscopy (XPS) analysis of NiO samples; the NiO sample that was deposited at an oxygen partial pressure of 5% shows the coexistence of Ni (852.8 keV) and NiO (854.3 keV) peaks. (d) Secondary-ion mass spectroscopy (SIMS) data (for the 5% oxygen partial pressure sample) showing the movement of O and Ni across the electrodes before and after electrical impulses.

highly controllable electrical pulse, which can overcome aforementioned problems, with regard to using the traditional nanostructures.

In this paper, we have applied NiO, which is a well-known resistance-switching material, to fabricate nanofilament channels that are electrically switchable and nonvolatile. We have also confirmed the properties of these filaments down to an extremely small size (a few nanometers).

Bistable resistance switching properties of NiO have previously been reported.[1,3,9,11] The NiO thin films used for our experiments were polycrystalline, as reported in previous works,[9] and the composition is believed to be coexisting metallic nickel and NiO in the bulk.[11] We fabricated ~20-nm-thick NiO thin films with ~100-nm-thick platinum top and bottom electrodes by reactive DC magnetron sputtering and atomic layer deposition (ALD), as described in detail in the Methods section of the Supporting Information. The NiO thin film with controlled nickel content provided the basis for electrical switching properties and controllable nanofilaments. Figure 1a shows the high-resolution transmission electron microscopy (HR-TEM) image of the polycrystalline NiO layers that show the electrical switching behavior. A highly ordered, stoichiometric structure can be seen in the TEM image of the grain interior. The grain-boundary region in the boxed area of Figure 1a was further studied by the inverse fast Fourier transform (IFFT) transmission electron microscopy (TEM) method, as shown in the left-hand side of Figure 1b. The composition analysis in the previous literature,[12] using electron energy-loss spectroscopy (EELS), verified the existence of a nickel-rich phase at these grain boundaries. This implies that the nanoscale filamentary paths that are made of nickel are formed as precipitates at the grain boundary, which is schematically depicted in the right-hand side of Figure 1b. This is further supported by the composition analysis by XPS and the secondary-ion mass spectroscopy (SIMS) methods, which verify the nickel-rich condition of NiO for the resistance switching; Figure 1c shows the XPS data for two NiO thin films formed via reactive sputtering. The sample that was deposited at an O_2 partial pressure of 5% exhibited bistable resistance switching, whereas the one grown with an O_2 partial pressure of 30% did not exhibit any stable resistance-switching phenomena. The most interesting feature in Figure 1c is the coexistence of a metallic nickel peak, at 852.8 eV, and a NiO peak, at 854.3 eV, for NiO samples deposited at an O_2 partial pressure of 5% (see Figure S1 in the Supporting Information). On the other hand, Figure 1d shows the SIMS results. It can be observed that the O atoms within the NiO layer diffuse out toward the platinum electrode after the electrical switching, indicating the nickel-rich condition in the NiO layer. The

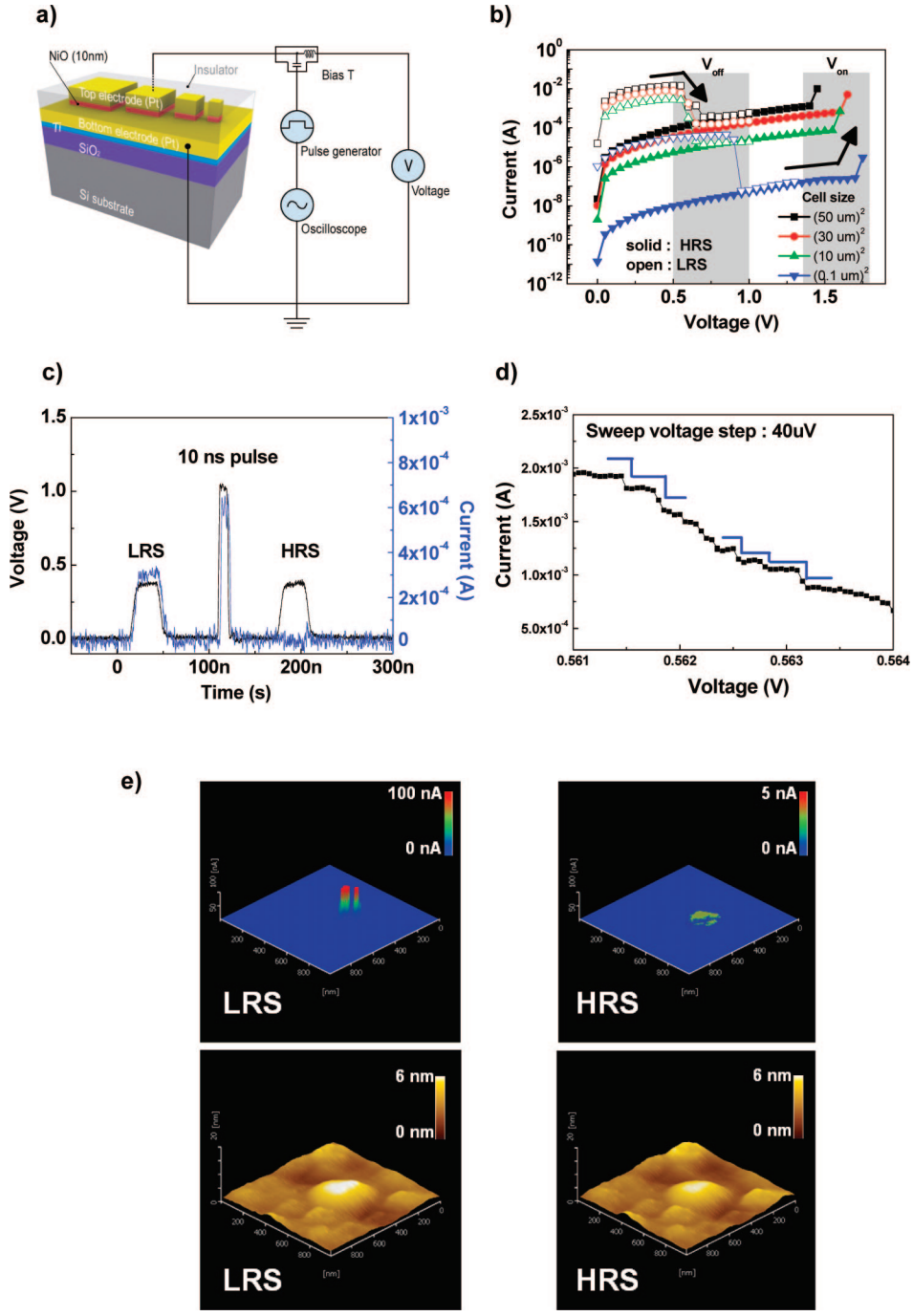

Figure 2. Experimental setup and switching characteristics. (a) Schematic diagram of the experimental setup and perspective view of our test cell structure. DC measurements are made using a semiconductor parameter analyzer; the pulse response is measured through an oscilloscope. (b) DC switching characteristics by cell area of Pt/NiO/Pt structures. (Application of an <1.5 V (V_{on}) voltage sweep is stopped by compliance current and switches the cell to the low-resistance state (LRS). Application of a 0.6–1.4 V (V_{off}) sweep returns the device to the high-resistance state (HRS).) (c) Switching speed of (0.1 μm)^2 cells. (A monitoring pulse is input before and after each 1 V switching pulse to examine the resistance change; typical switching speeds at this size were verified to be <10 ns.) (d) Discontinuous current response at small voltage increments. (The sweep range is 0.561−0.564 V, and the step was 40 μV. Switching of individual nanofilaments can be observed electrically.) (e) CS-AFM (top) and the corresponding topographical AFM images (bottom) of cell in the LRS and HRS states. (Control over the formation and destruction of nanofilament current paths is done by biasing the CS-AFM tip).

high initial nickel content in this sample should have played an important role in forming the switchable nanofilaments.[11] Reference 13 shows that the diffusion of Ni vacancies near the grain boundaries is significantly enhanced over the bulk. Therefore, it is believed that Ni atoms moving along these grain boundaries provide the necessary atoms to form the conducting network across the electrodes.

Control over the nanofilaments was attained by varying the input power across the electrodes. We used various electrode sizes from (50 μm)^2 to (0.1 μm)^2, as shown in the experimental schematic diagram of Figure 2a, to determine the effect of input power on the properties of as-formed nanofilaments. The results of DC sweep applied across the two electrodes are shown in Figure 2b for different electrode

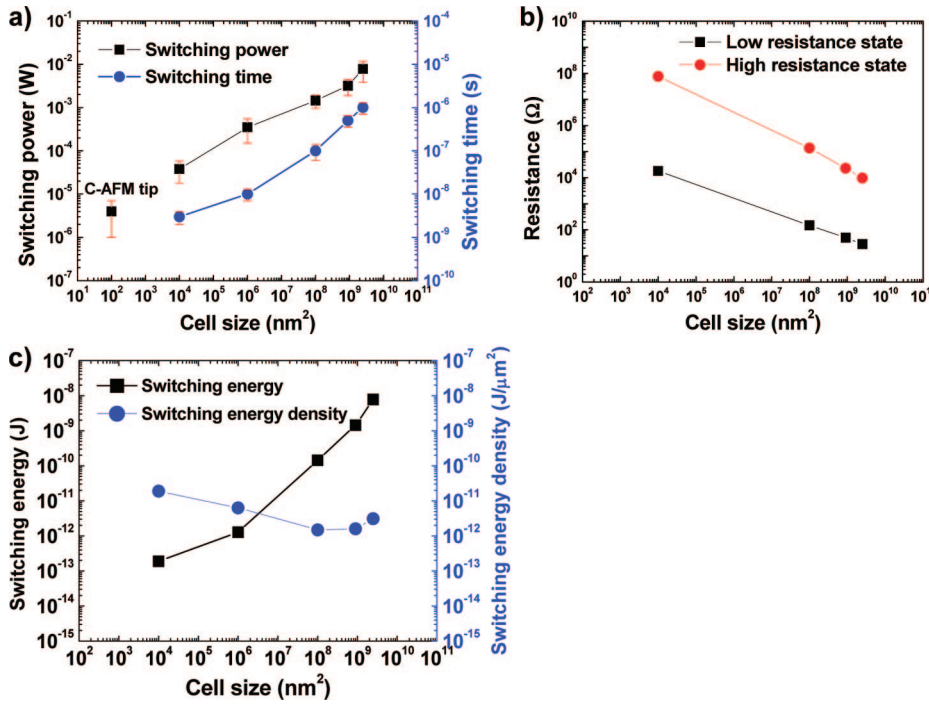

Figure 3. Switching speed and input power by cell size. (a) Cell size versus switching power and speed: power is calculated based on measurements from the LRS state to the HRS state by taking the product of maximum current and applied voltage. The error bar at the each node size is determined by the standard deviation of 5−10 successive measurements. The vertical error bars are experimental uncertainties that are due to the distribution of the switching operation. An additional data point for the CS-AFM results is shown at $(10\ \text{nm})^2$. (b) Cell size versus respective HRS and LRS resistance values, measured at a bias of 0.5 V. (c) Cell size versus switching energy and area energy density (switching energy is the product of switching time and power, as given in panel (a); each value is averaged over several measurements of switching from the LRS state to the HRS state at each size. The energy is given as the product of power and switching time, whereas the energy density is defined as the input energy divided by the cell size.

sizes. We define V_{on} as the voltage at which the NiO thin films transform from the high-resistance state (HRS) to the low-resistance state (LRS) and V_{off} as the voltage that starts the reverse process. I_{off} and I_{on} are defined as the respective current values at V_{off} and V_{on} just before resistance switching occurs. The nanofilaments can be switched to either HRS or LRS states by applying a unipolar voltage, which is more advantageous in high-density memory applications, because of simplified circuit architecture. Because of the rapid switching times of <10 ns of $(0.1\ \mu\text{m})^2$ cells, direct observation of the resistance change was not feasible with a long single pulse. Instead, the switching was confirmed by the monitoring pulses of 0.4 V applied before and after the 1 V, 10 ns switching pulse, as shown in Figure 2c. (Also see Figure S2 in the Supporting Information.) A more precise DC measurement at smaller voltage increments (step voltage of 40 μV) shows that the disconnection of individual nanofilaments occurs over several points in the cell, as observed from the steps in Figure 2d. Figure 2e shows the current map using a current-sensing atomic force microscopy (CS-AFM) system and the corresponding topographical images of LRS and HRS. One can observe that the nanoscale conducting paths appear in the LRS and disappear in the HRS.

The resistance switching in NiO can be understood based on the conductive filamentary path model,[1,3,14,15] in which the LRS of NiO thin films is due to conducting filamentary paths, presumably nickel nanowires at the grain boundaries (for supporting evidence, see Figure S3 in the Supporting Information). Figure 3a shows the relationship between the NiO cell size and the input switching power (left *y*-axis) from LRS to HRS that was calculated as $I_{off} \times V_{off}$ measured using the oscilloscope. The corresponding switching time is also presented in Figure 3a (right *y*-axis). Figure 3b shows that the resistance of the LRS increases as the area is reduced. This implies that the resistivity of the individual filament increases or the total cross-sectional area of filaments formed under a top electrode decreases as the cell size decreases. Considering the reduced switching time for smaller cells, the increased resistivity of the individual filament may result from the incomplete change in the individual filament. On the other hand, the decreased area of filaments means that fewer and/or thinner filaments were formed at small cell sizes. The reduction in the number of the filaments alone cannot account for the reduction in switching time with decreasing cell size in Figure 3a; if individual filaments are similar in size or resistivity and only the number of filaments varies between different node areas, the switching time should be insensitive to the node area, because filaments are connected in parallel circuits and, as such, ruptured independently. Therefore, the filaments should be thinner or have larger resistivity (be weaker) for the smaller electrode size.

Microscopically, the change from low resistance to high resistance is generally regarded as the oxidation process of the metallic nickel filaments;[16] thermally activated O atoms electromigrate to the anode side and oxidize the filament

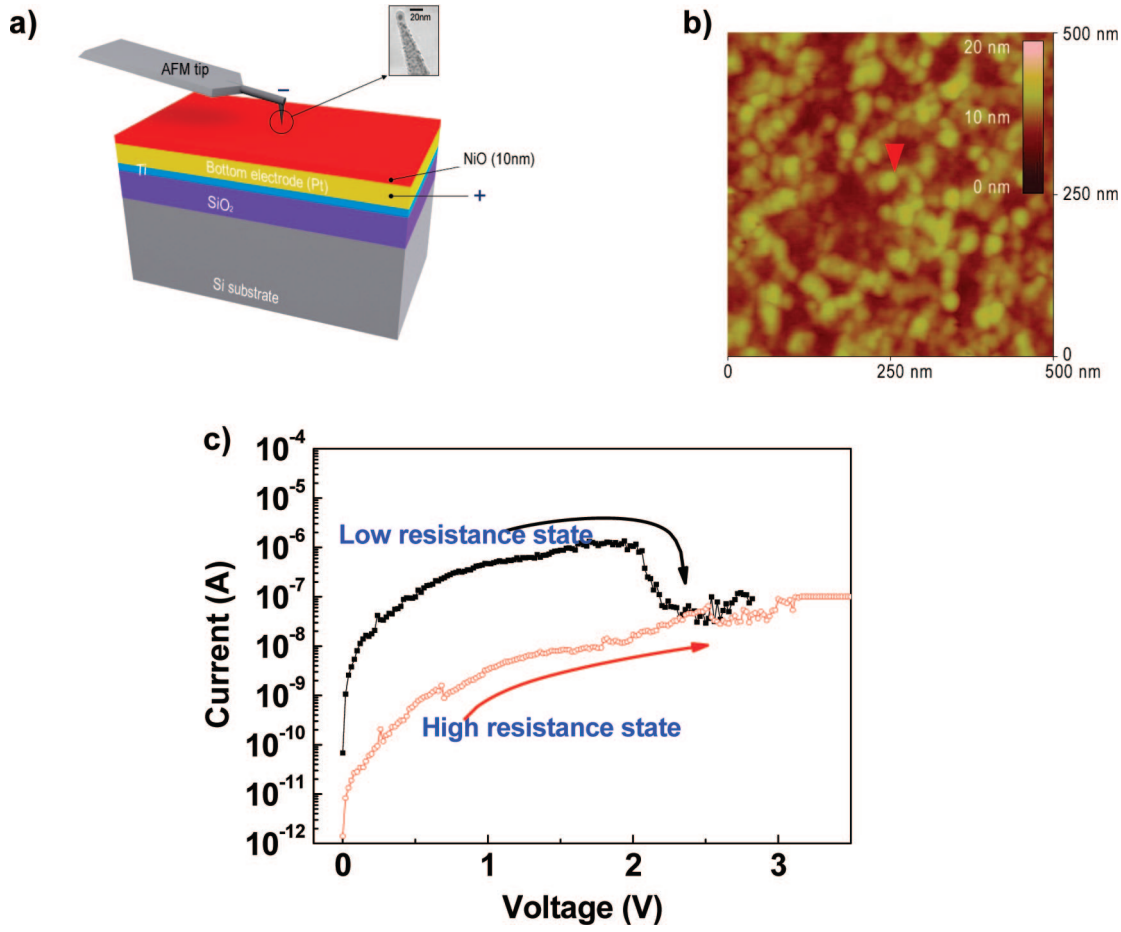

Figure 4. Resistance switching of ALD-deposited NiO with a 10-nm-diameter cell size. (a) Schematic illustration of the CS-AFM experimental set up for measuring the resistance switching of $(10\ \text{nm})^2$ cell size. Inset shows a scanning electron microscopy (SEM) image of an AFM tip with a curvature radius of 10 nm. (b) AFM scan image of the NiO surface; electrical switching measurements were formed at the grain boundary indicated by the red arrowhead. (c) Switching characteristics of CS-AFM, with a platinum-coated tip used as an electrode: maximum switching current was ~1 μA, and the switching power was ~2 μW. The "cell size" was approximated to be the AFM tip curvature of 10 nm.

locally. In the case of the bipolar switching, the migration of the oxygen vacancy affects the Schottky barrier.[17] Because the oxidization of filaments proceeds from the outer part, the switching time is reduced for thinner or weaker filaments, consistently with data in Figure 3a. It is also noticeable in Figure 3a that the switching time tends to saturate at small node areas. This can be explained based on the thermal energies. The oxidation process requires the diffusion of O atoms over the migration barriers. For instance, we have calculated the migration barrier of an O atom diffusing via the vacancy mechanism and found activation energies of 2−3 eV, depending on the charge states of the oxygen vacancy. (The computational setup follows ref 18. For more details, see Figure S4 in the Supporting Information.) This indicates that the thermal energy is critical for electromigration, within the short time scale required for the device operation. This energy is generated from Joule heating at the contact region between the electrode and filaments, where the resistance is presumably highest. As shown in Figure 3a, the power scales with the node area. Therefore, the local temperature around the filament is lower in small node areas and results in the observed saturation of the switching time.

Experimental data for critical switching energy is shown in Figure 3c. The switching energy (left y-axis) was calculated as the product of input power and switching time for each cell size. We verified that the switching speed was independent of NiO thickness for sample thicknesses in the range of 70−300 Å. Therefore, we believe that the switching mechanism occurs very locally, such that the total oxide thickness does not enter as a factor during resistance switching. The right y-axis shows the area energy density (switching energy/cell area, E/A) required for switching. There are slight variations in the area energy density, with $\sim 2 \times 10^{-12}$ J/μm^2 for cells larger than $(10\ \mu\text{m})^2$ and $\sim 2 \times 10^{-11}$ J/μm^2 for the smallest cell at $(0.1\ \mu\text{m})^2$. The variation is likely to be caused by second-order effects, including variation of filament paths and high-field edge effects, such that the actual scaling of the energy density should be closer to a constant. More-exact values for area energy density should be given as

$$\text{area energy density} = E \times \frac{y}{A}$$

where y is a factor that corrects for the number of filament paths by cell size, as mentioned earlier in Sato's work,[14] and

the thermal effects on filament size (or strength) discussed previously.

Further studies were performed by CS-AFM with a platinum-coated silicon tip to switch deposited NiO. A diagram of the experimental method is shown in Figure 4a. The CS-AFM tip has a diameter of 10 nm, and we were able to obtain filamentary paths within the NiO thin films using this method. Bistable resistance switching characteristics of the CS-AFM technique have been reported elsewhere.[15] Figure 4b shows a surface scan by AFM, and the red arrow in the figure indicates the grain boundary at which measurements were performed. By controlling the CS-AFM tip position precisely, electrical resistance switching between grain boundaries has been demonstrated, as shown in Figure 4c. The switching power given by CS-AFM is calculated by experimental measurements done with the CS-AFM system to be $\sim 2 \times 10^{-6}$ W/(10 nm)^2. The switching power is shown as an additional data point in Figure 3a, which is determined to be consistent with the behavior of other data. It would be intriguing to estimate the "ultimate" switching energy for smallest cell sizes. As a rough approximation, the results of Figure 3c were extrapolated down to "molecular" dimensions of $\sim$0.5 nm $\times$ $\sim$0.5 nm, which corresponds to the smallest nickel nanowires. The switching energy is predicted to be tens of electron volts, which is on the same scale of migration energy of O atoms (see previous discussion). This corroborates the assumption that the reset process is the oxidation of metallic filaments through the electromigration of O atoms.

In conclusion, we have demonstrated the fabrication of nanofilament nickel channels across two electrodes by electrical means. The nanoscale conducting paths formed at the grain boundaries of an insulating oxide matrix represent a promising element to be used in the resistance-based nonvolatile memories. The scaling behaviors of the nickel nanofilaments were examined, and the switching time was observed to decrease for smaller node areas, presumably because of the formation of thinner or weaker filaments. The reduction in the switching power for small cell sizes indicates that the nanofilament-based memory is also promising for low-power applications. The scaling behavior implies that, for the ultimate size of the nickel nanofilament, the resistance switching can be explained based on the binding-dissociation model at the atomic or molecular level.

Acknowledgment. S.H. and B.H.P. were supported in part by the National Program for 0.1 Terabit NVM Devices and Quantum Metamaterials Research Center. S.H.J. and B.H.P. were supported in part by the KOSEF NRL Program grant funded by the Korea Government MEST (No. R0A-2008-000-20052-0) and WCU program through the KOSEF funded by the MEST (No. R31-2008-000-10057-0).

Supporting Information Available: Further experimental details, electrical measurements, switching speed, low temperature behavior, and first-principles calculations of oxygen migration energy in NiO. (PDF) This material is available free of charge via the Internet at http://pubs.acs.org.

References

(1) Shima, H.; Takano, F.; Akinaga, H.; Tamai, Y.; Inoue, I. H.; Takagi, H. *Appl. Phys. Lett.* **2007**, *91*, 012901.
(2) Moller, S.; Perlov, C.; Jackson, W.; Taussig, C.; Forrest, S. R. *Nature* **2003**, *426*, 166.
(3) Lee, M. J.; Seo, S.; Kim, D. C.; Ahn, S. E.; Seo, D. H.; Yoo, I. K.; Baek, I. G.; Kim, D. S.; Byun, I. S.; Kim, S. H.; Hwang, I. R.; Kim, J. S.; Jeon, S. H.; Park, B. H. *Adv. Mater.* **2007**, *19*, 73.
(4) Dong, Y.; Yu, G.; McAlpine, M. C.; Lu, W.; Lieber, C. M. *Nano Lett.* **2008**, *8*, 386.
(5) Tans, S. J.; Verschueren, A. R. M.; Dekker, C. *Nature* **1998**, *393*, 49.
(6) Gudiksen, M. S.; Lauhon, L. J.; Wang, J.; Smith, D. C.; Lieber, C. M. *Nature* **2002**, *415*, 617.
(7) Ichihashi, T.; Fujita, J.; Ishida, M.; Ochiai, Y. *Phys. Rev. Lett.* **2004**, *92*, 215702.
(8) Mijatovic, D.; Eijkel, J. C. T.; Berg, A. *Lab Chip* **2005**, *5*, 492.
(9) Seo, S.; Lee, M. J.; Seo, D. H.; Jeoung, E. J.; Suh, D.-S.; Joung, Y. S.; Yoo, I. K.; Hwang, I. R.; Kim, S. H.; Byun, I. S.; Kim, J.-S.; Choi, J. S.; Park, B. H. *Appl. Phys. Lett.* **2004**, *85*, 5655.
(10) Hwang, D.-K.; Kang, S.-H.; Lim, J.-H.; Yang, E.-J.; Oh, J.-Y.; Yang, J.-H.; Park, S.-J. *Appl. Phys. Lett.* **2005**, *86*, 222101.
(11) Lee, M. J.; Park, Y.; Ahn, S. E.; Kang, B. S.; Lee, C. B.; Kim, K. H.; Xianyu, W. X.; Yoo, I. K.; Lee, J. H.; Chung, S. J.; Kim, Y. H.; Lee, C. S.; Choi, K. N.; Chung, K. S. *J. Appl. Phys.* **2008**, *103*, 013706.
(12) Park, G.-S.; Li, X.-S.; Kim, D.-C.; Jung, R.-J.; Lee, M.-J.; Seo, S. *Appl. Phys. Lett.* **2007**, *91*, 222103.
(13) Karakasidis, T.; Meyer, M. *Phys. Rev. B* **1997**, *55*, 13853.
(14) Sato, Y.; Kinoshita, K.; Aoki, M.; Sugiyama, Y. *Appl. Phys. Lett.* **2007**, *90*, 033503.
(15) Yun, J.-B.; Kim, S.; Seo, S.; Lee, M.-J.; Kim, D.-C.; Ahn, S.-E.; Park, Y.; Kim, J.; Shin, H. *Phys. Stat. Solidi* **2007**, *1*, 280.
(16) Kinoshita, K.; Tamura, T.; Aoki, M.; Sugiyama, Y.; Tanaka, H. *Appl. Phys. Lett.* **2006**, *89*, 103509.
(17) Jeon, S. H.; Park, B. H.; Lee, J.; Lee, B.; Han, S. *Appl. Phys. Lett.* **2006**, *89*, 042904.
(18) Park, S.; Ahn, H.-S.; Lee, C.-K.; Kim, H.; Jin, H.; Lee, H.-S.; Seo, S.; Yu, J.; Han, S. *Phys. Rev. B* **2008**, *77*, 134103.

NL803387Q